RSC Advances

PAPER

View Article Online
View Journal | View Issue

Cite this: *RSC Adv.*, 2022, **12**, 5557

Reduced graphene oxide-incorporated calcium phosphate cements with pulsed electromagnetic fields for bone regeneration†

Hoon Seonwoo,‡[ab] Han-Wool Choung,‡[c] Sangbae Park,‡[d] Kyoung Soon Choi,[e] Kyoung-Je Jang,[fg] Jangho Kim,[hi] Ki-Taek Lim,[j] Yeonju Kim,[k] Pankaj Garg,[l] Shambhavi Pandey,[l] Juo Lee,[bm] Joo-Cheol Park,[c] Yun-Hoon Choung,[k] Pill-Hoon Choung,[n] Soo Young Kim *[o] and Jong Hoon Chung *[lpqr]

Natural calcium phosphate cements (CPCs) derived from sintered animal bone have been investigated to treat bone defects, but their low mechanical strength remains a critical limitation. Graphene improves the mechanical properties of scaffolds and promotes higher osteoinduction. To this end, reduced graphene oxide-incorporated natural calcium phosphate cements (RGO-CPCs) are fabricated for reinforcement of CPCs' characteristics. Pulsed electromagnetic fields (PEMFs) were additionally applied to RGO-CPCs to promote osteogenic differentiation ability. The fabricated RGO-CPCs show distinct surface properties and chemical properties according to the RGO concentration. The RGO-CPCs' mechanical properties are significantly increased compared to CPCs owing to chemical bonding between RGO and CPCs. In *in vitro* studies using a mouse osteoblast cell line and rat-derived adipose stem cells, RGO-CPCs are not severely toxic to either cell type. Cell migration study, western blotting, immunocytochemistry, and alizarin red staining assay reveal that osteoinductivity as well as osteoconductivity of RGO-CPCs was highly increased. In *in vivo* study, RGO-CPCs not only promoted bone ingrowth but also enhanced osteogenic differentiation of stem cells. Application of PEMFs enhanced the osteogenic differentiation of stem cells. RGO-CPCs with PEMFs can overcome the flaws of previously developed natural CPCs and are anticipated to open the gate to clinical application for bone repair and regeneration.

Received 27th July 2021
Accepted 25th January 2022

DOI: 10.1039/d1ra05717k

rsc.li/rsc-advances

[a]*Department of Covergent Biosystems Engineering, College of Life Science and Natural Resources, Sunchon National University, Suncheon, 57922, Republic of Korea*

[b]*Interdisciplinary Program in IT-Bio Convergence System, Sunchon National University, Suncheon, 57922, Republic of Korea. E-mail: uhun906@gmail.com*

[c]*Department of Oral Histology-Developmental Biology, Dental Research Institute and School of Dentistry, Seoul National University, Seoul 03080, Republic of Korea. E-mail: woolmania@naver.com; jcapark@snu.ac.kr*

[d]*Department of Biosystems & Biomaterials Science and Engineering, Seoul National University, Seoul 08826, Republic of Korea. E-mail: sb92park@snu.ac.kr*

[e]*Advanced Nano-Surface Research Group, Korea Basic Science Institute, Daejeon 34133, Republic of Korea. E-mail: hanlalai@naver.com*

[f]*Division of Agro-System Engineering, College of Agriculture and Life Science, Gyeongsang National University, Jinju 52828, Republic of Korea. E-mail: kj_jang@gnu.ac.kr*

[g]*Institute of Agriculture & Life Science, Gyeongsang National University, Jinju 52828, Republic of Korea*

[h]*Department of Rural and Biosystems Engineering, Chonnam National University, Gwangju 500-757, Republic of Korea. E-mail: rain2000@jnu.ac.kr*

[i]*Interdisciplinary Program in IT-Bio Convergence System, Chonnam National University, Gwangju, 61186, Republic of Korea*

[j]*Department of Biosystems Engineering, Kangwon National University, Chuncheon, 24341, Republic of Korea. E-mail: ktlim@kangwon.ac.kr*

[k]*Department of Otolaryngology, Ajou University School of Medicine, Suwon 16499, Republic of Korea. E-mail: yeonju0130@naver.com; yhc@ajou.ac.kr*

[l]*Research Institute of Agriculture and Life Sciences, Seoul National University, Seoul 08826, Republic of Korea. E-mail: pnkjchem@gmail.com; shambhavi16@gmail.com*

[m]*Department of Animal Science & Technology, Sunchon National University, Suncheon, 57922, Republic of Korea. E-mail: dlwndh10@hanmail.net*

[n]*Department of Oral and Maxillofacial Surgery and Dental Research Institute, School of Dentistry, Seoul National University, Seoul 03080, Republic of Korea. E-mail: facial1004@gmail.com*

[o]*School of Chemical Engineering and Materials Science, Chung-Ang University, Seoul 06974, Republic of Korea. E-mail: sooyoungkim@cau.ac.kr*

[p]*Department of Biosystems Engineering, Seoul National University, Seoul 08826, Republic of Korea. E-mail: jchung@snu.ac.kr*

[q]*BK21 Global Smart Farm Educational Research Center, Seoul National University, Seoul 08826, Korea*

[r]*Convergence Major in Global Smart Farm, Seoul National University, Seoul 08826, Korea*

† Electronic supplementary information (ESI) available. See DOI: 10.1039/d1ra05717k

‡ These authors contributed equally to this study.

Introduction

Bone cements, which fill in bone defects and rapidly harden inside the defects, are widely used to heal the increasing number of physio-pathologic bone defects due to the aging population. Currently, polymethylmethacrylates (PMMA) are the most frequently used substance in clinical application because they have *in situ* setting ability and good mechanical properties.[1] However, due to the lack of bioactivity, PMMA cannot be degraded, in other words, they have neither osteoconductivity nor osteoinductivity. Moreover, their high hardening temperature, over 100°, causes necrosis of cells. Although *N*-butyl-2-cyanoacrylate (BCA)[2] and 2-octylcyanoacrylate (OCA)[3] were developed to resolve this problem, their biological inactivity remains a critical problem. To complement these weaknesses, calcium phosphate cements (CPCs) were developed. Because CPCs have similar chemical components with native bone, they are bioresorbable, resulting in easy substitution by native tissues. They also have good osteoconductivity and low setting temperature.[4] To date, synthetic calcium phosphate (CaP) biomaterials and bioactive glasses, *i.e.*, hydroxyapatite (HA), dicalcium phosphate (DCP) and α or β-tricalcium phosphate (α or β-TCP) have been utilized as bone substitutes.[5–11] In addition, natural sources, *e.g.*, sintered animal bones and clamshells, were also used in CPCs due to their similarity with native human bone. They frequently used porcine,[12] bovine,[13] chicken,[14] and horse bone.[15,16] However, CPCs still have serious problems: their mechanical strength is low, which is a critical flaw for use in clinical applications. Thus, many researchers attempt to promote the mechanical strength of CPCs. The mechanical strength of CPCs is deeply related with the micro/nanostructure of the particle size, for instance, porosity,[17] crystal size,[18] powder distribution,[19,20] and nano/micro CaP particle composition.[21] The addition of additives, *e.g.*, chitosan (CS), citric acid,[22] cellulose,[23] and fiber,[24] significantly improved the mechanical properties, as well. However, those methods has not been used in fabricating CPCs using CaP particles derived from natural source, called natural CPCs. Therefore, an easier and more effective method to reinforce the mechanical properties of natural CPCs should be developed. Moreover, because CPCs are regarded to have low osteoinductivity, a better solution to improve osteoinductivity of CPCs is prerequisite.

Graphene, discovered experimentally in 2004, consists of a two-dimensional (2D) honeycomb lattice structure of carbon.[25] Graphene has many subtypes depending on the fabrication method, for example, graphene made by chemical vapor deposition (CVD),[26] graphene nanoribbon (GNR),[27] graphene oxide (GO),[28] and reduced graphene oxide (RGO).[29] Its good biological properties – interaction with RNA and DNA, cellular adhesion, cellular uptake, antibacterial ability, and good biodegradability – led to its application in the biological field. In tissue engineering, graphene has been used in two ways: (1) stem cell engineering and (2) strengthening the mechanical properties of scaffolds. First, graphene/GO was involved in osteogenesis,[30] epithelial genesis,[28] and neurogenesis[31] of mesenchymal stem cells (MSCs) and neurogenesis

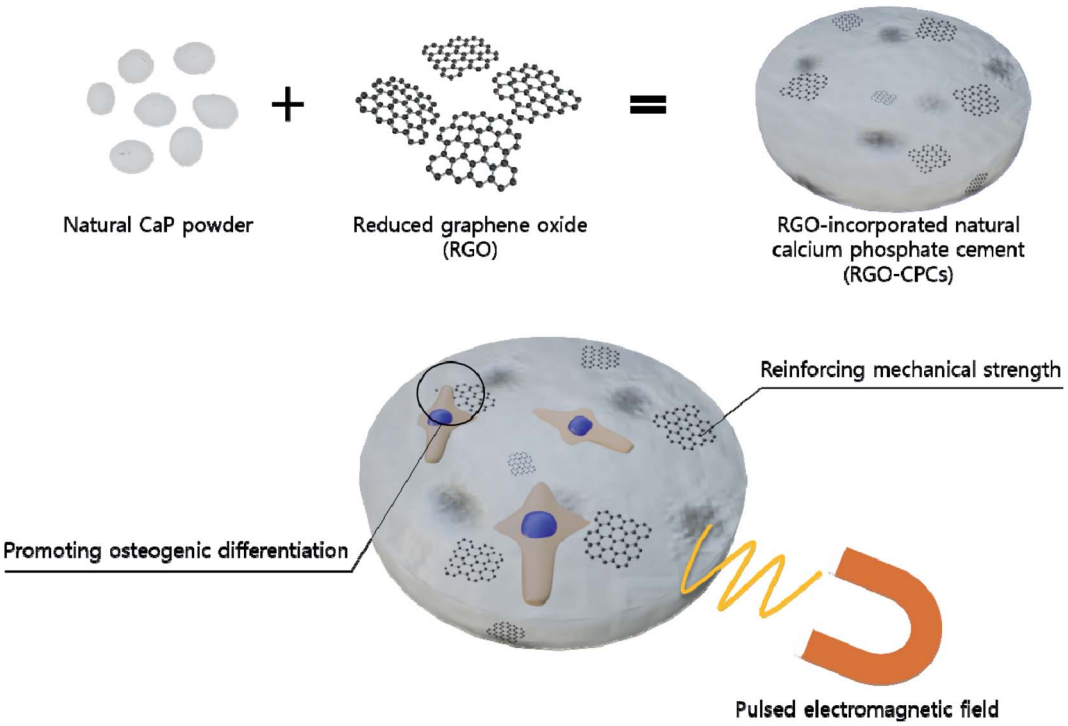

Fig. 1 Schematic diagram of the research concept. Natural CaP powder and RGO were thoroughly mixed. Then, the mixed powder was hardened by CS solution to fabricate RGO-CPCs. The RGO in RGO-CPCs is expected to reinforce the mechanical properties and improve osteogenic differentiation, which would contribute to better bone regeneration. Pulsed electromagnetic fields were exerted on the RGO-CPCs for the promotion of synergic effects. CaP: calcium phosphate, CS: chitosan.

of neural stem cells (NSCs).[32] Furthermore, GO-CaP nanocomposite synergically enhanced osteogenic differentiation of MSCs.[33] Secondly, graphene has been used to enhance the mechanical properties of tissue-engineered scaffolds. Yang *et al.* reported that the elastic modulus and maximum tensile strength were enhanced by the addition of GO.[34] Baradaran *et al.* and Fan *et al.* also reported that the mechanical strength of HA-RGO and HA-GO nanocomposites was improved compared with HA composite.[35,36] These two properties – acceleration of osteogenic differentiation and reinforcement of mechanical strength – can also be utilized in natural CPCs. Furthermore, the electrical functionality of graphene is applied to stem cell engineering. The combination of RGO and pulsed electromagnetic fields (PEMFs) increased ECM formation, membrane proteins, and metabolism, resulting in enhanced osteogenic and neurogenic differentiation.[37,38] Simultaneous application of graphene and PEMFs can make synergic effects on bone regeneration.

Consequently, we hypothesized that if we incorporate graphene in natural CPCs, we could reinforce the mechanical properties as well as the osteogenic differentiation and osteoconductivity of natural CPCs (Fig. 1). Therefore, we fabricated graphene-incorporated natural CPCs and evaluated their various properties.[39,40] In order to utilize electrical characteristics of graphene, PEMFs were applied to the graphene-incorporated CPCs. As a graphene ingredient, RGO was chosen because of its several advantages – easy synthesis and easy incorporation. At first, their characteristics, *e.g.*, morphological, chemical, and mechanical properties, were analyzed. *In vitro* study was conducted with preosteoblast cell line (MC3T3-E1) and mesenchymal stem cells (rat-derived adipose stem cells, rASCs). Their cytotoxicity, viability, and adhesion were analyzed. Then, a migration assay was assessed to verify the osteoconductivity. Their osteogenic differentiation was evaluated by western blot, immunocytochemistry (ICC), and alizarin red staining (ARS). Their efficacy was evaluated by *in vivo* study with and without stem cells, suggesting that RGO-reinforced CPC (RGO-CPC) is a promising tool for clinical application. Finally, the synergic potential of RGO-CPCs with PEMFs were investigated.

Materials and methods

Fabrication of RGO-CPCs

The preparation method for micro/nano-sized natural bone powders followed the preliminary study.[21] Briefly, horse bones (Jejushopping, Republic of Korea) were soaked in distilled water to drain the remaining blood for 24 hours. Then, the bones were immersed in hydrogen peroxide (Duksan Chemicals Co, Korea) for 72 hours. After soaking, the flesh on surface was cut out, and the horse bones were sintered in an electric furnace (UP350E, Yokogawa Co, Japan) at 1200 °C for 2 hours. The sintered bones were ground into powders using a miller (A10, IKA-WERKE, Japan) and the ground bone powders were sintered three more times. Micro-sized horse bone powders of which the particle size was below 100 μm were collected by sieve (Daihan Scientific, Korea). Nano-sized horse bone powders were ground by a Nano Sizer Fine Mill (Deaga Powder Systems Co. Ltd, Republic of Korea), a device that pulverizes and disperses particles by friction between beads and a revolving screen. The collected micro/nano-sized powders were mixed 50 : 50 (w/w) and RGO was incorporated into the powders by 10 000 : 1, 1000 : 1, and 100 : 1 (w/w). The resultant concentrations of RGO were 0, 0.01, 0.1, and 1 wt%, respectively. A 3.5% chitosan (CS) solution for hardening CPCs was prepared by dissolving chitosan (molecular weight: 200 000, D: 90%, Taehoon Co, Korea) in 2% lactic acid (v/v, #50215, Duksan Chemicals Co, Korea) solution. The prepared powders and CS solution were thoroughly mixed with ratios of 0.45 : 1 (v/w) and placed into a polydimethylsiloxane (PDMS) mold (6 φ diameter, 2 mm height) at 37 °C and 100% humidity for 4 hours. The fabricated RGO-CPCs were classified following the RGO concentration in powders. Detailed information is listed in Table 1.

Table 1 NOMENCLATURE of experimental group

Abbreviation	Bone powder	RGO (%, w/w)	3.5% CS sol. (w/v)
No RGO	O	—	0.45
0.01% RGO	O	0.01	0.45
0.1% RGO	O	0.1	0.45
1% RGO	O	1	0.45

Characterization

The fabricated CPCs were dried completely at room temperature, and observed by a field emission scanning electron microscope (FESEM, SUPRA 55VP, Carl Zeiss, Germany). The presence of crystalline phases on the RGO-CPCs according to bone powder and RGO was XRD and Raman spectroscopy. In XRD, an X-ray diffractometer (New D8 advanced XRD, Bruker, Germany) with copper Kα radiation at 40 kV and 40 mA was used. The samples were scanned from 20 to 65° using steps of 2 theta with a counting time of 60 s per step. The crystalline phase compositions were identified with reference to standard JCPDS cards available in the system software. The Raman spectra of the RGO-CPC was obtained with a T64000 (Horiba Jobin Yvon) at an excitation wavelength of 514.54 nm. XPS was conducted on a Sigma Probe (ThermoVG, U.K.) operating at a base pressure of 5×10^{-10} mbar at 300 K with a nonmonochromatized Al Kα line at 1486.6 eV, a spherical sector analyzer of 180°, a mean diameter of 275 mm, an analysis area of 15 μm to 400 μm, and multichannel detectors. The mechanical properties of the RGO-CPCs were analyzed using a texture analyzer (TAXT2i, Stable Microsystems Co, US). The prepared CPCs samples (6 φ diameter, 2 mm height) were compressed at a crosshead speed of 1 mm min^{-1} until failure, and the stress–strain diagram of the samples were recorded. From the diagrams, the elastic modulus, maximum allowable strain, and maximum compressive stress were calculated.

In vitro study

A mouse calvaria-derived osteoblast cell line, MC3T3-E1 (CRL-2593, ATCC, USA) was cultured in proliferation media. The

proliferation medium was α-MEM (#LM 008-02, WELGENE Inc., Korea) supplemented with 10% fetal bovine serum (FBS, #SH30919.03, Hyclone, USA), 1% antibiotics (#LS 203-01, WELGENE Inc., Korea) at 37 °C in 5% CO_2 conditions. The media was changed every other day. To isolate rASCs, subcutaneous fat tissues (2 mL volume) in the operation site were obtained from a rat. Tissues were washed with phosphate buffered saline (PBS; Gibco, Milan, Italy), digested with 100 U mL^{-1} collagenase type I (Sigma-Aldrich, St. Louis, MO) in low glucose Dulbecco's modified Eagle's medium (DMEM; Gibco-BRL, Grand Island, NY), and incubated for 8 hours to lyse the adipose tissues. The stromal fraction was collected by centrifugation and then passed through a cell strainer (100 mL size) to remove any large cell clumps and particles. For the cell culture and expansion of adipose-derived cells, cells were grown in low glucose DMEM with 10% fetal bovine serum (FBS; Gibco, Milan, Italy) and 1% penicillin–streptomycin (Gibco, Milan, Italy) at 37 °C in a 5% CO_2 atmosphere. To confirm the phenotypic characterization of the rASCs, undifferentiated cells were cultured in stromal DMEM media. If the cells were more than 80% confluent, the cells were harvested using trypsin–EDTA and resuspended at a concentration of 1×10^6 cells per ml in fluorescence activated cell sorting (FACS) buffer. Cells were firstly stained using fluorescein isothiocyanate (FITC)-conjugated antibody CD105 (mesenchymal stem cell marker) for 1 h at 4 °C and FACS was performed using FACS DiVa software (BD Bio-sciences, San Jose, CA).

A concentration of 1×10^4 cells per well MC3T3-E1 and rASCs were seeded on 96-well plate and incubated at 37 °C in a 5% CO_2 atmosphere for 1 day. RGO-CPCs were put into another 96 well plate. They were immersed in 200 μl culture media and incubated at 37 °C in a 5% CO_2 atmosphere for 24 h. After soaking, the culture media were collected. Then, cell-cultured media were removed and the collected culture media from the RGO-CPCs were added to the plate and incubated for 12 and 24 h. Following the incubation, the cytotoxicity was measured by WST-1 (EZ-Cytox Cell Viability Assay Kit, EZ3000 Daeillab Service Co., Seoul, Republic of Korea). Each RGO-CPC was added to a 96 well plate. 1×10^4 cells per well MC3T3-E1 and rASCs were seeded on RGO-CPCs and incubated at 37 °C in a 5% CO_2 atmosphere for 6 h. Following the incubation, media were removed and PBS were added to the wells to gently wash out unattached cells. After washing, fresh media were added to the wells and the cell adhesion was measured by WST-1 (EZ-Cytox Cell Viability Assay Kit, EZ3000 Daeillab Service Co., Seoul, Republic of Korea). For immunocytochemistry (ICC), MC3T3-E1 and rASCs (1×10^4 cells per sample) were seeded onto RGO-CPCs, and allowed to spread for 1 or 7 days in culture media at 37 °C in a humidified atmosphere containing 5% CO_2. Adhered cells were fixed with a 4% paraformaldehyde solution (Sigma-Aldrich, Milwaukee, WI) for 20 min, permeabilized with 0.2% Triton X-100 (Sigma-Aldrich, WI, Milwaukee) for 15 min, and stained with TRITC-conjugated phalloidin (Millipore, Billerica, MA) and 4,6-diamidino-2-phrnykinodole (DAPI; Millipore, Billerica, MA) for 1 h. Focal adhesions (FAs) were stained with a monoclonal anti-vinculin antibody (1 : 100; Millipore, Billerica, MA) and an FITC-conjugated goat anti-mouse secondary antibody (1 : 500; Millipore, Billerica, MA). Images of the stained cells were taken using a confocal laser scanning microscope (LSM710, Carl Zeiss, Germany). Each RGO-CPC was added to a 96 well plate, and 1×10^4 cells per well MC3T3-E1 and rASCs were seeded on the RGO-CPCs and incubated at 37 °C in a 5% CO_2 atmosphere for 1, 3, or 7 days. Following the incubation, cell viability was measured by WST-1 (EZ-Cytox Cell Viability Assay Kit, EZ3000 Daeillab Service Co., Seoul, Republic of Korea).

The total cellular protein was extracted by RIPA lysis buffer (62.5 mM Tris–HCL, 2% SDS, 10% glycero, pH 7.5) with added proteinase inhibitor cocktail (Invitrogen, USA). Cell lysates were incubated on ice for 30 min and then centrifuged at 13 000 rpm for 30 min at 4 °C. Supernatant (protein lysate) was collected and the protein concentration was determined by a micro bicinchoninic acid (BCA) Protein Assay Kit (Bio-rad, Hercules, Calif). Twenty five μg-aliquots of the cell lysates were separated by 8% SDS-PAGE under reducing conditions. Separated proteins were transferred to a PVDF membrane (Millipore Corporation, Bedford, MA, USA) at 30 V for 1 h. After blocking with 5% skim milk in PBST, the membranes were incubated overnight in primary antibody at 4 °C. Then, the primary antibody was removed and washed thrice by PBST for 10 min each. After washing, samples were incubated with a secondary antibody for 2 h at room temperature. After incubation, the secondary antibody was removed and washed thrice using PBST for 10 min. Anti-alkalinephosphatase (ALP, ab354, Abcam, Cambridge, MA, USA), Runt-related transcription factor-2 (Runx-2, ab23981, Abcam, Cambridge, MA, USA), and osteocalcin (OCN, AB10911, Millipore, USA) were used as the primary antibodies and horse raddish peroxidase (HRP)-conjugated anti-rabbit immunoglobulin G (G21234, Invitrogen, USA) was used as the secondary antibody. Quantification of the western blot was performed using the Image J software with a normalization of the level of the entire protein. MC3T3-E1 and rASCs were fed with α-MEM and DMEM media to which 50 μg mL^{-1} ascorbate-2-phosphate (Sigma-Aldrich, WI, Milwaukee) and 10 μM dexamethasone (Sigma-Aldrich, WI, Milwaukee) were added for 2, 3, and 4 weeks, respectively. Calcium precipitation of the ECM was visualized by staining with ARS (Sigma-Aldrich, WI, Milwaukee). Briefly, the ethanol-fixed cells and matrix were stained for 1 hour with 40 mM ARS (pH 4.2) and extensively rinsed with water. After photography, the bound stain was eluted with 10% (wt/vol) cetylpyridinium chloride, and the ARS in samples was quantified by measuring the absorbance at 544 nm.

In vivo study

A second animal model using rat calvarial defects was designed to evaluate the effects of RGO-CPCs on regeneration capacities of bony structures without transplantation of cells. All experiments using mice and rats were approved by the Seoul National University Institutional Animal Care and Use Committee (SNU-120427-2-2). 0% and 0.01% RGO-CPCs were implanted into critical-size calvarial defects in twelve Sprague Dawley rats. 8 mm diameter bony defects were made, and copious irrigation

with sterile saline and hemostasis was performed. The critical-size defects in the control group received only a blood clot as a negative control, and Bio-Oss powder was used as a positive control. Sample harvesting was performed after 8 weeks. To evaluate the effects of RGO-CPCs on mineralized tissue formation of mesenchymal stem cells *in vivo*, human alveolar bone marrow stem cells (hABMSCs, 2.5×10^4 cells) were pre-seeded on 0% and 1% RGO-CPCs disk (diameter of 6 mm), incubated for 4 hours, and then transplanted into the subcutaneous spaces of immunocompromised mice (NIH-bg-nu/nu-xid, Harlan Sprague Dawley, Indianapolis, IN, USA). We collected human alveolar bone tissues at Seoul National University Dental Hospital (Seoul, Korea). The experimental protocol was approved by the Institutional Review Board. Informed consent was obtained from the patients. Human ABMSCs which were inserted into polycaprolactone tube (diameter of 3 mm) were used as a negative control, and the cells mixed with Bio-Oss (Ed Geistlich Sons, Wolhusen, Switzerland) powder, a bovine bone derivative, as a positive control for transplantation. Samples ($n = 5$) were obtained after 12 weeks. The transplanted hABMSCs samples and the calvarial segments were dissected carefully and samples were immersed in 4% paraformaldehyde then kept for an additional 24 hours. After being decalcified in a 10% EDTA (pH 7.4) solution, the specimens were embedded in paraffin. Serial 5 μm thick sections were cut and stained with hematoxylin/eosin (H/E) for histological analysis. For immunohistochemistry, transplanted hABMSCs samples were incubated overnight at 4 °C with rabbit polyclonal bone sialoprotein (BSP) (SC-59772, Santa Cruz Biotechnology) antibody at a dilution of 1 : 200. Sections were then incubated with secondary antibodies, anti-rabbit IgG, at room temperature for 30 min and reacted with the avidin–biotin–peroxidase complex (Vector Laboratory, Burlingame, CA). Signals were converted using a DAB kit (Vector Laboratory). Hematoxylin was used for staining of nuclei.

Application of PEMFs on RGO-CPCs

Electromagnetic stimulation was applied on RGO-CPCs. Their efficacy was evaluated *via* ARS. rASCs were fed with α-MEM and DMEM media to which 50 μg mL^{-1} ascorbate-2-phosphate (Sigma-Aldrich, WI, Milwaukee) and 10 μM dexamethasone (Sigma-Aldrich, WI, Milwaukee) were added for 2, 3, and 4 weeks, respectively. The PEMFs were irradiated using a solenoid. Electric signals, of which condition was square wave, ±5 V, 50 Hz-frequency, and 50%-duty cycle, were generated using a function generator. The condition of resultant PEMFs was 0.6 ± 0.05 mT with 50 Hz and expose time on samples was 30 minutes per day. Calcium precipitation of the ECM was visualized by staining with ARS (Sigma-Aldrich, WI, Milwaukee). Briefly, the ethanol-fixed cells and matrix were stained for 1 hour with 40 mM ARS (pH 4.2) and extensively rinsed with water. After photography, the bound stain was eluted with 10% (wt/vol) cetylpyridinium chloride, and the ARS in samples was quantified by measuring the absorbance at 544 nm.

Statistical analysis

Statistical analyses were performed using the Statistical Analysis System (SAS) for Windows Ver. 9.4 (SAS Institute). The least significant difference (LSD) method and unpaired Student's *t*-tests were used to compare the means of the properties of the RGO-CPCs. The level of significance was $p < 0.05$.

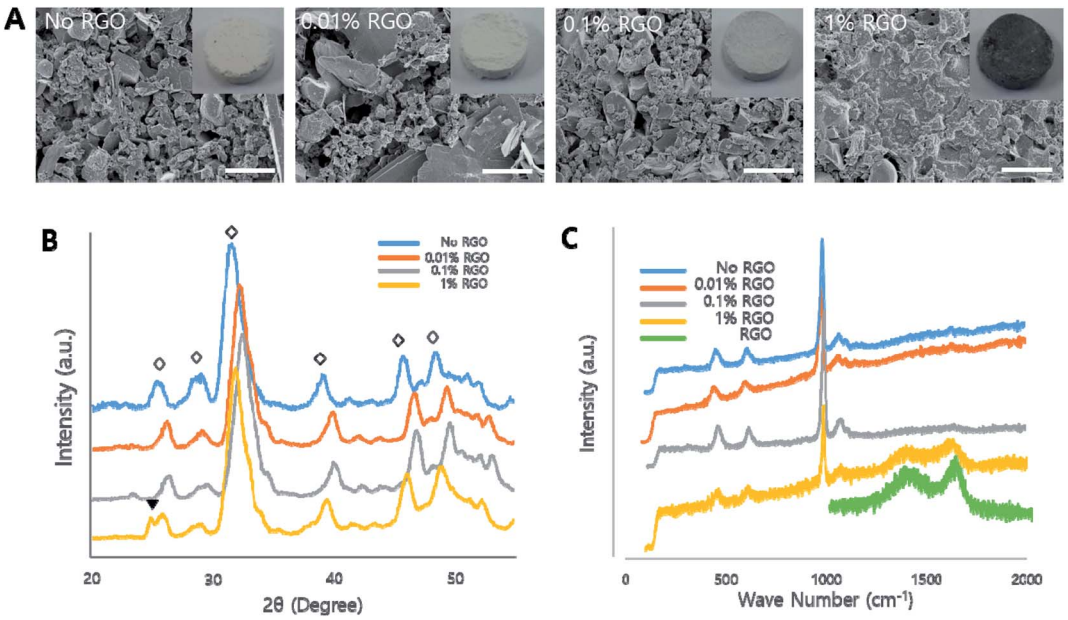

Fig. 2 Characteristics of RGO-CPCs (A) morphological analysis. RGO-CPCs became darker as the RGO concentration increased (inset). According to the FESEM results, the surface of RGO-CPCs aggregated more with the increased RGO concentration. Scale bars = 3 μm. (B) XRD results. HA specific peaks were present in all samples. In 0.1 and 1% RGO, new peak representing RGO was present at approximately 25°. (C) Raman spectroscopy results. Hydroxyapatite specific peaks were shown in all samples. The peaks representing RGO were clearly shown in 1% RGO. FESEM: field emission scanning electron microscopy, XRD: X-ray diffraction.

Results

Characteristics of RGO-CPCs

To investigate the effects of RGO on the characteristics of CPCs, the morphological, chemical, and mechanical characteristics were evaluated to reveal the influence of RGO on natural CPCs. In this study, four groups, *e.g.*, no, 0.01%, 0.1% and 1% RGO were investigated (Table 1). We first examined their morphology. As the inset of Fig. 2A indicated, CPCs became darker with increasing of RGO. According to the scanning electron microscopy (SEM), their microstructural morphology became smoother as the RGO concentration increased. (Fig. 2A) energy-dispersive X-ray spectroscopy (EDS) evaluated the presence of graphene (Fig. S1†). All samples showed carbon peak because CS, having carbon in its back bone, was in all samples. Then, we examined the chemical properties of RGO-CPCs. In the X-ray diffraction (XRD) results, peaks were present at 25.4, 28.96, 31.38, 39.06, 45.76, and 48.6°, showing typical peaks of crystal structure of HA in CPCs.[41] (Fig. 2B). Further, at approximately 25° the peaks representing RGO were shown on 1% RGO. In the Raman spectroscopy, all samples exhibited representative HA peaks (Fig. 2C). Further, 1% RGO had 1398 (D) and 1696 (G) peaks, verifying the presence of RGO.

We next examined mechanical properties of RGO-CPCs (Fig. 3A). The elastic modulus of 0.1% and 1% RGO were

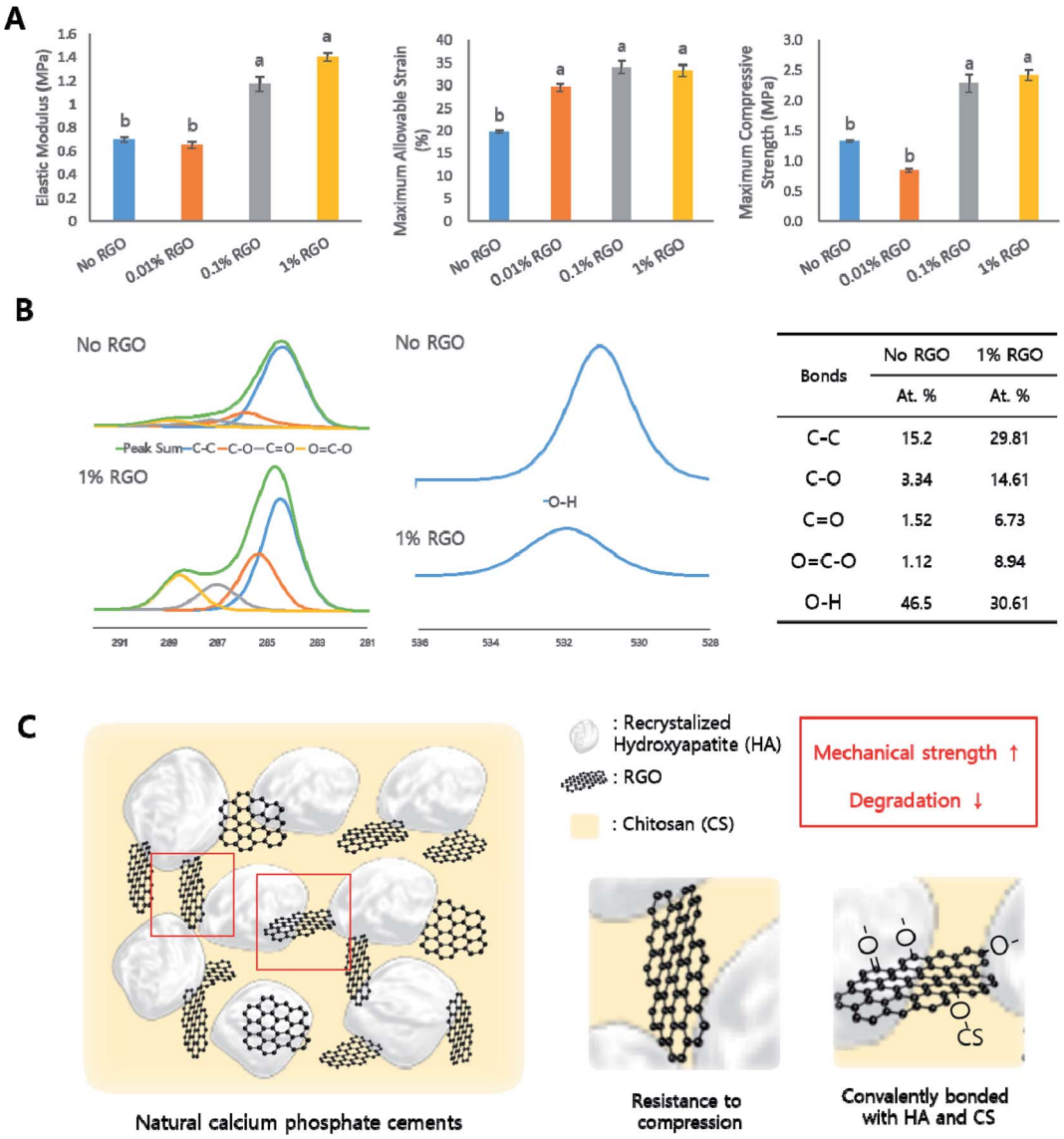

Fig. 3 Mechanical properties of RGO-CPCs. (A) Mechanical properties (elastic modulus, maximum allowable strain, and maximum compressive stress) of RGO-CPCs immediately after fabrication. Elastic modulus and maximum compressive stress of 0.1 and 1% RGO were significantly enhanced and the maximum allowable strain of all RGO-CPCs was increased compared to No RGO. ($n = 10$, LSD) (B) XPS results. C 1s peaks of 1% RGO representing C–C, C–O, C═O, and O═C–O bonding increased compared to No RGO. Whereas, an O 1s peak representing O–H bonding decreased, indicating covalent bonding may occurred. (C) Possible mechanism of RGO-CPCs. Covalent bonding between HA, CS, and RGO as well as high mechanical properties of RGO would result in the reinforcement of mechanical properties. XPS: X-ray photoelectron scopy, HA: hydroxyapatite, CS: chitosan.

Table 2 XPS results of RGO-CPCs

	No RGO			0.1% RGO		
Bonds	Peak BE (eV)	FWHM (eV)	At. %	Peak BE (eV)	FWHM (eV)	At. %
C–C	284.47	1.85	38.24	284.51	1.74	26.21
C–O	286.35	1.85	5.72	285.89	1.74	23.94
C═O	288.27	1.85	6.41	287.25	1.91	6.02
O═C–O	—	—	—	288.45	1.91	4.69
O–H	531.11	2	26.03	531.01	1.96	7.47
H_2O	532.29	2	7.45	532.3	1.96	23.48
N–H	398.81	1.4	0.67	398.99	1.87	4.9
Ca(HA)	347.09	1.83	10.47	347.11	1.93	2.29
P–O	132.58	1.52	5.02	132.67	1.6	0.98

significantly increased compared to No RGO. The maximum allowable strains of the RGO-CPCs were all increased, and the maximum compressive strength of 0.1 and 1% RGO were significantly increased compared with No RGO. To reveal the long-term behavior of RGO-CPCs in the human body, a soaking test was assessed by immersing the RGO-CPCs into simulated body fluid (SBF), and their mass and mechanical properties were analyzed per every week (Fig. S3†). The mass of the RGO-CPCs was steadily decreased (not significantly), whereas the mechanical properties of the RGO-CPCs were gradually increased. In week 3, all of the mechanical properties of 0.1% RGO were excessively increased. In accordance with these results, it was concluded that incorporation of RGO in CPCs highly strengthened the mechanical properties of RGO-CPCs. For verifying the chemical reaction, X-ray photoelectron spectroscopy (XPS) was conducted on GO, RGO, No RGO CPC and 1% RGO CPC (Fig. 3B and S2†). In Fig. 3B, all C 1s peaks representing C–C, C–O, C═O, and O═C–O bonding highly increased on 1% RGO whereas an O 1s peak on No RGO representing O–H bonding highly decreased. Furthermore, XPS is also assessed on No and 0.1% RGO soaked in SBF for 3 weeks. As a result, a C 1s peak representing C–O bonding highly increased while an O 1s peak representing O–H bonding highly decreased (Table 2).

In vitro study on MC3T3-E1

Next, several *in vitro* studies were performed to evaluate whether RGO-CPCs are appropriate for bone tissue engineering. We first used preosteoblastic MC3T3-E1 cells to determine the efficacy of RGO-CPCs on differentiation of osteoblasts. First, in the cytotoxicity test, RGO-CPCs denoted slight toxicity at 12 h (Fig. 4A). However, their toxicity became marginal at 24 h. In the cell adhesion test, the cell adhesion rate was significantly decreased in 1% RGO at 24 h (Fig. 4B, inset). To determine the reason for decrease, ICC to stain the vinculin, the protein related with focal adhesion, was conducted (Fig. 4C). On day 1, expression of vinculin decreased according to the increase of RGO. Nonetheless, the expression was increased in all RGO-CPCs on day 7, suggesting that the adverse effect of RGO on focal adhesion diminished with long-term cell adhesion. In the cell viability test, the optical density of the RGO-CPCs steadily decreased with the increase of RGO (Fig. 4B). Next, we conducted an osteogenic differentiation study of RGO-CPCs. First, protein expressions related with osteogenesis were checked by western blot. (Fig. S4A and B†) Runt-related transcription factor 2 (Runx-2), intermediated osteogenic marker, and osteocalcin (OCN), late osteogenic marker, were upregulated faster in 1% RGO, whereas alkaline phosphatase (ALP), early osteogenic marker, showed marginal results among all samples. In the ICC, consistent with the western blot results, higher expression of OCN was observed on 1% RGO. (Fig. S4C†) Furthermore, ARS was conducted to determine the calcium deposition. The highest calcium deposition rate was shown on 1% RGO. (Fig. S4D and E†).

In vitro study on rASCs

Our data showed that RGO-CPCs promoted osteoblastic differentiation of preosteoblastic MC3T3-E1 cells. Therefore, we next explored various *in vitro* studies with rASCs, one of the mesenchymal stem cells, including the ability of stem cell differentiation of RGO-CPCs. There was no different cytotoxicity between CPCs and RGO-CPCs at 12 h. In contrast, the cytotoxicity of RGO-CPCs was decreased at 24 h (Fig. 5A). The cell adhesion rates of rASCs were not significant comparatively with No RGO, except for 1% RGO (Fig. 5B). ICC was investigated to evaluate the vinculin expression of rASCs on RGO-CPCs (Fig. 5D). Consistent with the cell adhesion rate, vinculin expression decreased with the increased graphene concentration. Cell viability was decreased with increased RGO (Fig. 5C). When conducting the differentiation study, RGO-CPCs accelerated osteogenic differentiation of rASCs (Fig. 6). In the western blotting and immunostaining results, the highest expression of OCN was recorded on 1% RGO (Fig. 6A–D). Analogous results were observed in ARS assay. At 4 weeks, rASCs on 1% RGO showed the best calcium deposition (Fig. 6E and F).

In vivo studies with or without hABMSCs

To evaluate whether RGO-CPCs could enhance bone regeneration under microenvironments of bony defects *in vivo*, 0% and 0.01% RGO-CPCs were implanted into critical sized defects of rat calvaria for twelve weeks (Fig. 7A). Bio-Oss™ was used as

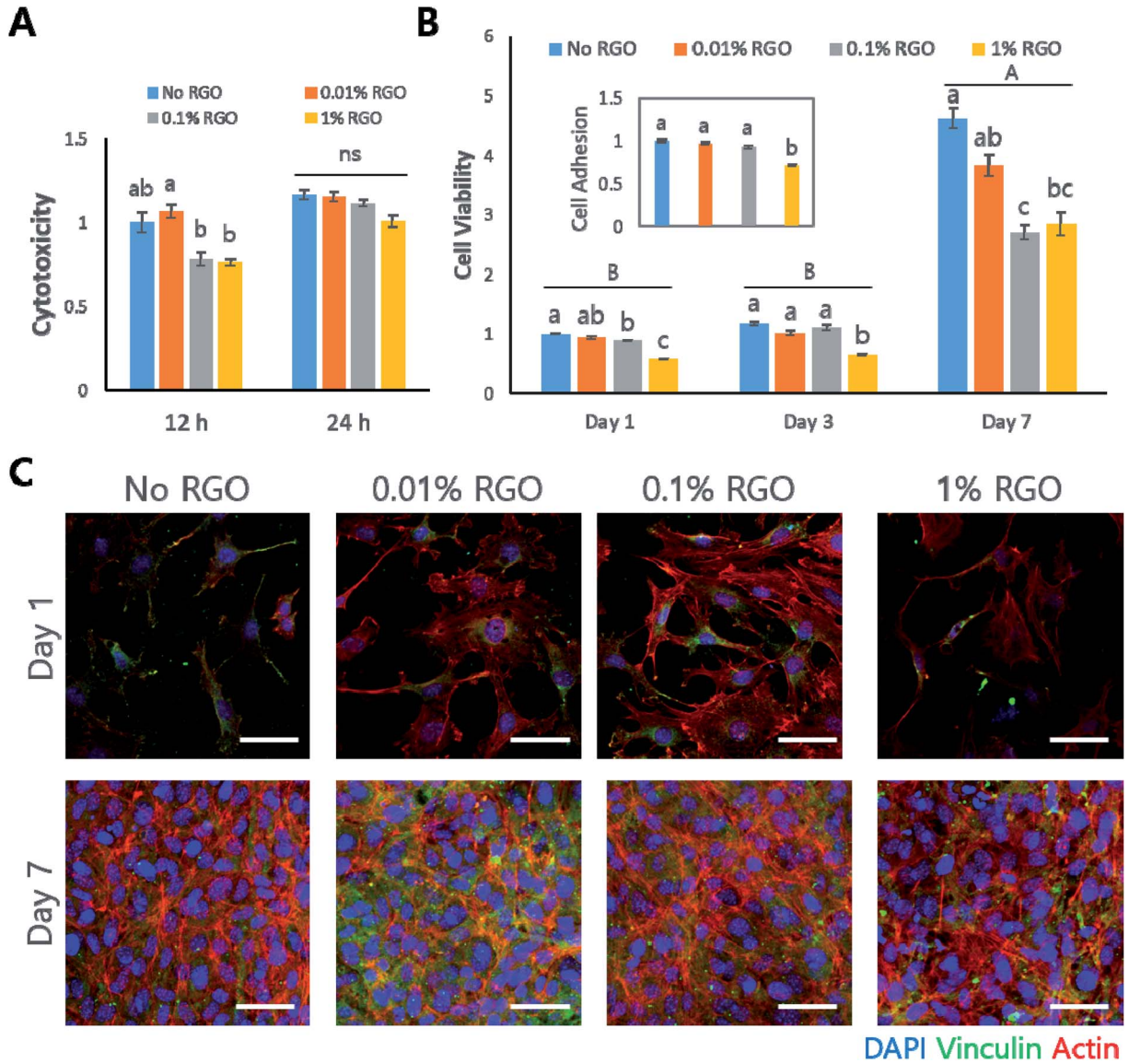

Fig. 4 *In vitro* study of MC3T3-E1. (A) Cytotoxicity result. The cytotoxicity of 0.01% RGO was the least at 12 hours, whereas the cytotoxicity of all CPCs was insignificant at 24 hours ($n = 5$). (B) Cell viability result. On day 7, the cell viability of 0.1 and 1% RGO decreased significantly compared with No RGO ($n = 5$, LSD). Inset: cell adhesion result. There is no significant difference except for 1% RGO ($n = 5$, LSD). (C) ICC results. Vinculin expression decreased with increased of 1% RGO. Scale bars = 50 μm. ICC: immunocytochemistry.

a positive control for bone regeneration. There was no evidence of inflammation in all groups. The calvarial defects in the control group showed formation of thin fibrous connective tissue layers and small amounts of bony growth at the margins of the defect, while the Bio-Oss™ group generated bone-like mineralized tissues on the border of Bio-Oss™ particles (Fig. 7B). In the 0.01% RGO, more amounts of newly-formed bone tissues were regenerated in the periphery of surrounding the bony defects compared to the 0% RGO. The regenerated mineralized tissues in the Bio-Oss and 0.01% RGO groups showed morphological characteristics of calvarial bone present at the margins of the defect, including typical osteocytes entrapped inside the matrix, and osteoblasts lining the outer margin of the mineralized tissue. These findings suggest that RGO-CPCs themselves could enhance bone regeneration without transplantation of any cells *in vivo*.

Based on the results from these *in vitro* experiments with mesenchymal stem cells, human alveolar bone marrow stem cells (hABMSCs)-seeded 0% and 1% RGO-CPCs disc were transplanted into immunocompromised mice subcutaneously to evaluate the effects of RGO-CPCs on osteoblast differentiation of mesenchymal stem cells (Fig. 7C). Harvested samples were stained with hematoxylin and eosin (H&E) and immunostained with bone sialoprotein (BSP) antibody twelve weeks after transplantation. Histological analysis revealed that the accumulation of extracellular matrices and collagen for generating mineralization foci were detected in the Bio-Oss™ and both RGO groups compared to the control group (Fig. 7D). 1%

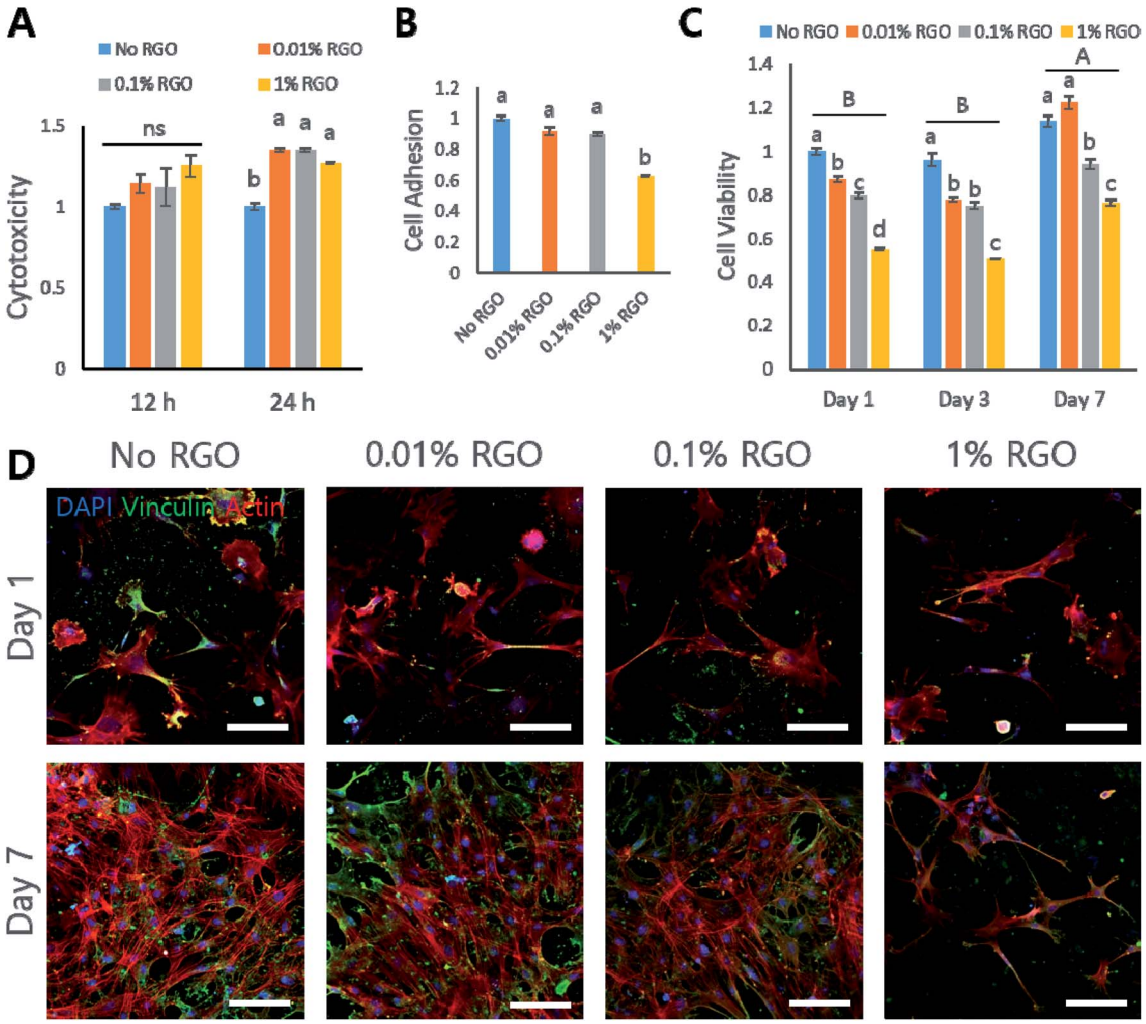

Fig. 5 *In vitro* study of rASCs. (A) Cytotoxicity result. The cytotoxicity of RGO-CPCs was lower than No RGO at 24 hours, whereas the cytotoxicity of all CPCs was insignificant at 12 hours ($n = 5$). (B) Cell adhesion result. There is no significant difference except for 1% RGO ($n = 5$, LSD). (C) Cell viability result. On day 7, the cell viability of 0.1 and 1% RGO significantly decreased compared with No RGO ($n = 5$, LSD). (D) ICC result. Vinculin expression decreased with increased 1% RGO. Scale bars = 100 μm. ICC: immunocytochemistry.

RGO displayed osteoblast-like cells with abundant matrix formation. BSP expression was observed in the Bio-Oss™ group but weakly in the control group. In the 1% RGO, the expression of BSP protein was detected in osteoblast-like cells that contact with the RGO-CPCs, however, there were few cells with BSP expression in the 0% RGO.

Application of PEMFs on RGO-CPCs

The efficacy of PEMFs on RGO-CPCs were investigated (Fig. 7E). The rASCs were seeded onto the No RGO and 1% RGO groups, and the PEMFs were exposed for 3 weeks. The result of calcium deposition was evaluated by ARS. On week 2, there's no significant difference among samples, whereas, on week 3, 1% RGO with PEMFs exhibited significant difference.

Discussion

CPCs have such good bioactivity that can be absorbed by surrounding tissue and be replaced with native tissues. However, the low mechanical strength of CPCs has remained a critical weakness.[4] There are a few methods to reinforce the mechanical properties of natural CPCs because the existing methods work properly only in CaP synthesis. Likewise, not only osteoconductivity, but better osteogenic differentiation is important for natural CPCs. Thus, in this study, RGO was incorporated into the horse bone-derived natural CPCs to alleviate the disadvantages.

Horse bone powders, RGO, and CS solution were mixed thoroughly following the above mentioned concentration (Table 1) and were hardened in polydimethylsiloxane (PDMS) molds. As shown in Fig. 2A, RGO-CPCs became darker with the increase of the RGO concentration and their surface became more coagulated with the increase of the RGO concentration. Next, the chemical characteristics of mixed powders were examined. In the XRD and Raman spectroscopy, specific peaks of RGO were also observed in RGO-CPCs (Fig. 2B and C). From the results, it was confirmed that the RGO was successfully incorporated in the RGO-CPCs. CPCs consist of one or more calcium

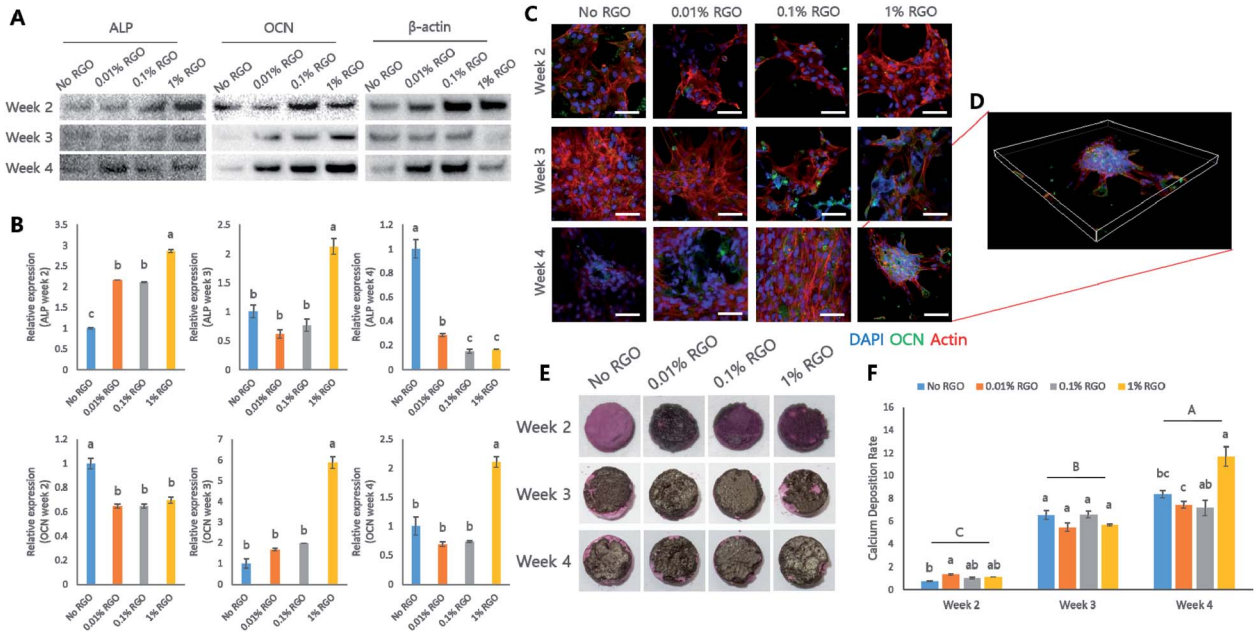

Fig. 6 Osteogenic differentiation study on rASCs (A) representative western blot result. ALP, OCN expressions were evaluated during 4 weeks. (B) The relative expressions of osteogenic marker protein were calculated. In weeks 2 and 3, ALP expression was increasingly promoted with increased RGO, indicating that the more RGO is incorporated, the faster the early stage of osteogenesis is. In weeks 3 and 4, OCN expression of 1% RGO was highly increased, indicating that 1% RGO underwent late stage osteogenesis earlier. (C) ICC result. OCN expression for 4 weeks is depicted. At 4 weeks, 1% RGO had the highest expression. Scale bars = 100 μm. (D) Three dimensional images of OCN expression on 1% RGO. Hemisphere-shaped cell aggregation indicates higher OCN expression. (E) Representative images of ARS. (F) Quantitative analysis of ARS. The calcium deposition rate of 1% RGO in week 4 had the highest value with a significant difference. (n = 5, LSD) ALP: alkaline phosphatase; OCN: osteocalcin, ICC: immunocytochemistry. ARS: alizarin red staining.

phosphate that can be mixed in a liquid form and hardened. During the setting reaction of CPC pastes, the *in situ* formation of the crystals of HA precipitate occurs. The crystalline structure of HA in CPCs was further confirmed by XRD results.[41] Next, the mechanical properties of the RGO-CPCs were measured (Fig. 3). For the 0.1% and 1% RGO, the mechanical properties were enhanced almost twice. Further, when soaked in SBF, 0.1% RGO showed outstanding improvements of mechanical properties. For RGO preparation, we first synthesized GO using modified Hummers' method. The GO was then reduced using hydrazine monohydrate to acquire RGO. In the XPS results of GO and RGO, the peaks representing oxygen functional groups in the RGO (C–O, C═O and C═O–O) were decreased compared to those of GO (Fig. S2†). However, the results still show small peaks representing C–O, C═O, and C═O–O owing to remaining oxygen functional groups after the hydrazine monohydrate reduction.[42] Therefore, oxygen containing functional groups in C 1s peaks might have increased with increasing RGO content (Fig. 3B). In the XPS results of CPC, it was confirmed that all C 1s peaks representing C–C, C–O, C═O, and O═C–O bonding are highly increased in 1% RGO whereas an O 1s peak representing O–H bonding highly decreased. The increase of C–C bonding is expected mainly due to the presence of RGO. Interestingly, other C 1s peaks exhibiting covalent bonding with oxygen were also increased owing to remaining oxygen functional groups in RGO whereas O–H bonding decreased, which implicates that the covalent bonding among RGO, CS, HA might happen. Thus, it is expected that the reinforcement of mechanical strength is due to covalent bonding between HA, CS, and RGO as well as the high mechanical properties of RGO (Fig. 3C). There were several reports that incorporation of or synthesis with GO enhanced the mechanical properties of HA and CS. The tensile strength and elastic modulus of GO/CS composite film were increased more than those of CS film.[34] The elastic modulus of GO/HA and the hardness of GO/HA/CS complex were evidently increased compared to HA.[43] Moreover, synthesis with HA and RGO improved the micro hardness, elastic modulus, and fracture toughness.[36] However, it has not been reported that the mixing and hardening of the HA/RGO/CS complex results in reinforcement of the mechanical properties of CPCs. Consequently, in our knowledge, this is the first report about the reinforcement of CPCs by the mixing of RGO/CS/HA composite. Together, this easy and simple method is highly suitable for application in natural CPCs. Hence, this method is expected to enlarge the application range of natural CPCs.

After investigation of the morphological, chemical, and mechanical properties of RGO-CPCs, their behaviors were examined by MC3T3-E1 and rASCs *in vitro*. The adhesion rate of RGO-CPCs decreased as the RGO concentration increased. This was visually confirmed by ICC of vinculin. As shown in Fig. 4C and 5D, vinculin expression decreased with the increase of the RGO concentration. From the cell viability result in Fig. 4B, the viability of MC3T3-E1 significantly increased in all experimental groups on day 7. Furthermore, the cell viability indicated that

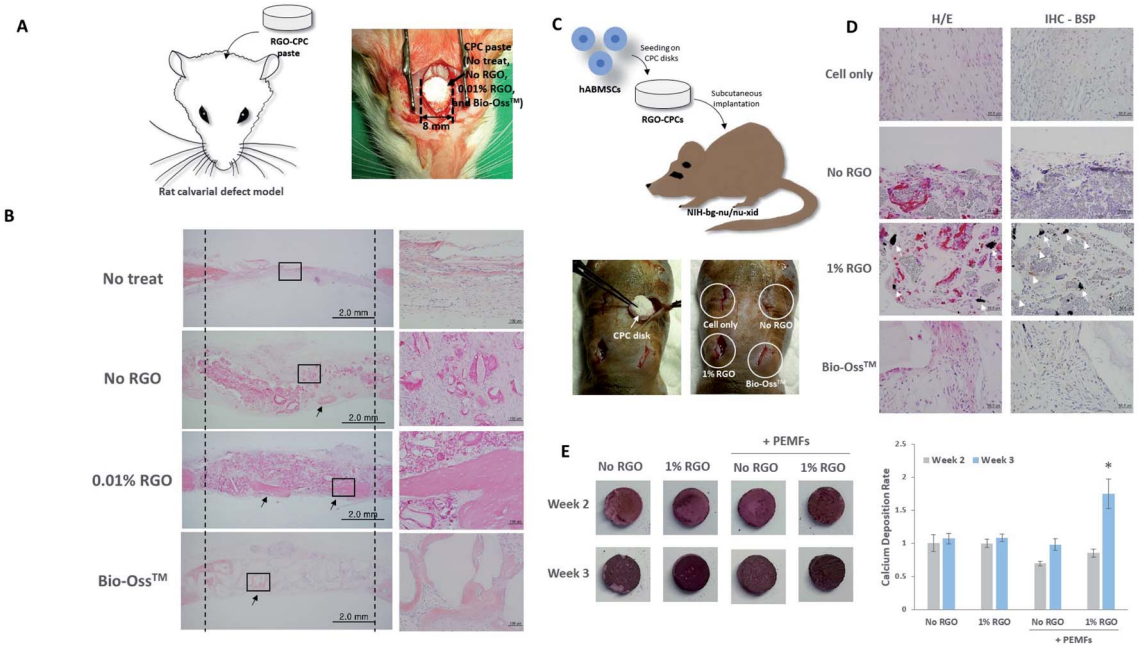

Fig. 7 *In vivo* study. (A) No RGO, 0.01% RGO, and Bio-Oss™ were applied on rat calvarial defect models. (B) Twelve weeks later, 0.01% RGO successfully induced bone ingrowth. (C) The osteogenic capability of RGO-CPCs was assessed. hABMSCs were seeded onto the RGO-CPCs and those were subcutaneously implanted in nude mice. (D) Twelve weeks later, the hABMSCs on 1% RGO is similar with osteoblast-like cells while osteogenic differentiation deemed to be delayed in other groups. Moreover, 1% RGO strongly expressed BSP. (E) ARS results of RGO-CPCs under PEMFs stimulation. (A) Representative results of ARS. (B) Quantitative results of ARS study. The PEMFs stimulation exhibited nonsignificant results on week 2 whilst the PEMFs stimulation induced significant result upon 1% RGO on week 3. hABMSCs, human alveolar bone marrow stem cells; PEMFs, pulsed electromagnetic fields.

the results decreased with increasing of RGO concentration. There are two possible causes: (1) RGO-CPCs have cytotoxicity or (2) RGO-CPCs make cells promote osteogenic differentiation, rather than cell proliferation or migration. Considering their cytotoxicity result, the cytotoxicity of RGO-CPCs is insignificant (Fig. 4A and 5A). Moreover, Tatavarty *et al.* reported that GO-CaP nanocomposite improved osteogenic differentiation of human mesenchymal stem cells (hMSCs)[44] and Li *et al.* reported that the chitosan–GO–HA composite enhanced osteogenesis of MG63.[43] Consequently, RGO-CPCs were anticipated to promote differentiation of the cells. As expected, RGO-CPCs enhanced osteogenic differentiation of MC3T3-E1 and rASCs. In week 2, 1% RGO most rapidly promoted early expression of ALP, the early marker of osteogenic differentiation (Fig. 6A). Subsequently, it promoted early expression of Runx-2 and OCN on week 3 and week 4, respectively. The results are consistent with the ICC and ARS results (Fig. 6C). The 1% RGO recorded the highest OCN expression and calcium deposition in week 4. Many researchers have been dedicated to enhance osteogenic capability of CPCs. According to the researches, it was reported that the addition of Arg–Gly–Asp (RGD), fibronectin, and platelet concentration enhanced osteogenesis of human umbilical cord mesenchymal stem cells (hUCMSCs).[45] However, addition of carbon-based materials in CPCs related with osteoinductivity was not investigated. Thus, it was revealed that the utilization of carbon-based materials in natural CPCs will simultaneously enhance the mechanical properties and osteoinductivity. Thus, RGO-CPCs are anticipated to open the gate for the clinical application for natural CPCs.

Based on the cell type, RGO-CPCs can be utilized differently. In the case of MC3T3-E1, 0.01% RGO showed the highest cell proliferation among the RGO CPC groups (Fig. 4B) whereas RGO-CPCs represented comparatively low osteogenic capability. Hence, 0.01% RGO is suitable for bone ingrowth, commonly used in orthopaedic application. In contrast, 1% RGO demonstrated more effective osteogenic differentiation of rASCs than other RGO-CPCs. Thus, for stem cell-based bone regeneration, incorporation of 1% RGO and stem cells simultaneously would be more effective. Thus, in *in vivo* study, 0.01% RGO is applied on rat calvarial defect model and 1% RGO was subcutaneously injected in immunocompromised mice with hABMSCs. As a result, No and 0.01% RGO promoted bone ingrowth compared to No treat and Bio-Oss™ (Fig. 7B). Particularly, bony structures were more observed on 0.01% RGO compared with No RGO, indicating that 0.01% RGO have better osteoconductivity than No RGO. Further, 0.01% RGO sustained their morphology whereas No RGO degraded much faster than 0.01% RGO. It seems that the delay of degradation of 0.01% RGO is due to chemical bonding between HA, CS, and RGO. The chemical bonding would not only hamper the collapse of transplanted area but also promote the fast migration of osteogenic precursor cells. In case of stem cell-based study, the 1% RGO promoted osteogenic differentiation of hABMSCs (Fig. 7D). The cells seeded on 1% RGO formed osteoblast-like shapes faster

than other groups. It was also revealed by immunohistochemistry (IHC) by staining BSP, the marker of osteogenesis.[46] The cells seeded on 1% RGO expressed BSP, whereas BSP is poorly expressed in other groups. Consistently with *in vitro* study, the efficacy of 1% RGO on osteogenesis of hABMSCs was confirmed obviously by *in vivo* study. The hABMSCs, extracted from human alveolar bone, frequently used in dento-alveolar bone regenerations,[47] that is, the RGO-CPCs have a potential to be used in dental as well as orthopaedic fields. Consequently, it is anticipated that 0.01% RGO is proper to be used in clinical applications for bone regeneration of defected area alone, because it is good for bone ingrowth. Further, 1% RGO is expected to be used in tissue engineering-based bone regeneration since it enhances osteogenesis of stem cells. Both 0.01% and 1% RGO would be applicable in clinical application.

The use of pure RGO instead of GO or functionalized RGO is notable in this study. There were several reports on the use of GO in synthesis with HA for reinforcement of mechanical properties.[35,48] Functionalized RGO[49] and RGO synthesized with HA[36] have been reported, as well. However, our research is, in our knowledge, the first report to use pure RGO in the study of CPCs. The use of pure RGO has several advantages: (1) ease of fabrication. Simple mixing results in the easy fabrication process maintaining the reinforced mechanical properties. (2) Better promotion of osteogenesis. Lee *et al.* reported osteogenic capability of graphene is better than GO.[30] Hence, RGO may promote better osteoinductivity than GO. (3) Good biodegradability. Lee *et al.* reported that RGO/HA composite never induced interleukin-6 and tumor necrosis factor-α, related with inflammatory response.[50] Hence, when conducting *in vivo* study, its toxicity is not a significant matter. (4) Utilization of the functionality of graphene. For example, exposure on graphene sheets could induce microelectric current.[51] It was anticipated that when RGO is incorporated in CPCs, microelectric current, which can cause synergistic effects on osteogenic differentiation, would be induced by exposure in electromagnetic field.[37] Fig. 7E confirmed the hypothesis about the synergic effects of graphene and microelectric current on bone regeneration. Furthermore, its unique properties, including high elastic modulus and thermal properties can be used in tissue regeneration. The incorporation of RGO on CPCs may provoke synergic effects in tissue engineering.

Conclusion

In this study, a new method to incorporate RGO into natural CPCs for reinforcing the mechanical properties, osteoconductivity and osteoinductivity simultaneously is developed for bone tissue engineering. RGO-CPCs had enhanced mechanical properties, including elastic modulus, maximum allowable strain, and maximum compressive strength. In the soaking test, the mechanical properties of the RGO-CPCs were enhanced in comparison with CPCs. Furthermore, the RGO-CPCs not only had good migration ability but also improved osteogenic differentiation of MC3T3-E1 and rASCs compared to CPCs. In *in vivo* study, bone regeneration and osteogenesis of RGO-CPCs also evaluated. In conclusion, the RGO-CPCs are expected to overcome the flaws of formerly developed CPCs and open the gate for clinical application in bone repair, regeneration, and bone tissue engineering.

Conflicts of interest

The authors declare that they have no known competing financial interests or personal relationships that could have appeared to influence the work reported in this paper.

Acknowledgements

This work was supported by the Technology Innovation Program (or Industrial Strategic technology development program, 20001590, Development of AI based hand prosthesis with more than 4 types of function through a patient specific osseointegrated implant development) funded by the Ministry of Trade, industry & Energy (MI, Korea). This research was supported by the MSIT (Ministry of Science and ICT), Korea, under the Grand Information Technology Research Center support program (IITP-2021-2020-0-01489) supervised by the IITP (Institute for Information & communications Technology Planning & Evaluation). This work was supported by the Korea Institute of Energy Technology Evaluation and Planning (KETEP) and the Ministry of Trade, Industry & Energy (MOTIE) of the Republic of Korea (No. 20194210100230). This work was supported by the Korea Institute of Energy Technology Evaluation and Planning (KETEP) and the Ministry of Trade, Industry & Energy (MOTIE) of the Republic of Korea (No. 20202020900060). This work was supported by the National Research Foundation of Korea (NRF) grant funded by the Korea government (MSIT) (NRF-2020R1F1A1067439).

References

1 B. Magnan, M. Bondi, T. Maluta, E. Samaila, L. Schirru and C. Dall'Oca, Acrylic bone cement: current concept review, *Musculoskelet. Surg.*, 2013, **97**(2), 93–100.
2 P. Maurer, K. Bekes, C. Gernhardt, H.-G. Schaller and J. Schubert, Comparison of the bond strength of selected adhesive dental systems to cortical bone under in vitro conditions, *ISO*, 2004, **33**(4), 377–381.
3 A. B. Brochu, G. A. Evans and W. M. Reichert, Mechanical and cytotoxicity testing of acrylic bone cement embedded with microencapsulated 2-octyl cyanoacrylate, *J. Biomed. Mater. Res., Part B*, 2014, **102**(1), 181–189.
4 J. Zhang, W. Liu, V. Schnitzler, F. Tancret and J.-M. Bouler, Calcium phosphate cements for bone substitution: chemistry, handling and mechanical properties, *Acta Biomater.*, 2014, **10**(3), 1035–1049.
5 L. C. Chow, M. Markovic and S. Takagi, A dual constant-composition titration system as an in vitro resorption model for comparing dissolution rates of calcium phosphate biomaterials, *J. Biomed. Mater. Res., Part B*, 2003, **65**(2), 245–251.
6 K.-J. Jang, S. Kim, S. Park, W. Kim, Y. Gwon, S. Park, K.-T. Lim, H. Seonwoo and J. Kim, Lithographically-

fabricated HA-incorporated PCL nanopatterned patch for tissue engineering, *Appl. Sci.*, 2020, **10**(7), 2398.

7 S. R. Meka, V. Agarwal and K. Chatterjee, In situ preparation of multicomponent polymer composite nanofibrous scaffolds with enhanced osteogenic and angiogenic activities, *Mater. Sci. Eng., C*, 2019, **94**, 565–579.

8 R. Soni, N. V. Kumar, S. Chameettachal, F. Pati and S. N. Rath, Synthesis and optimization of PCL-bioactive glass composite scaffold for bone tissue engineering, *Mater. Today: Proc.*, 2019, **15**, 294–299.

9 S. R. Meka, S. Kumar Verma, V. Agarwal and K. Chatterjee, In situ silication of polymer nanofibers to engineer multi-biofunctional composites, *ChemistrySelect*, 2018, **3**(13), 3762–3773.

10 D. Meng, S. N. Rath, N. Mordan, V. Salih, U. Kneser and A. R. Boccaccini, In vitro evaluation of 45S5 Bioglass®-derived glass-ceramic scaffolds coated with carbon nanotubes, *J. Biomed. Mater. Res., Part A*, 2011, **99**(3), 435–444.

11 M. Shaltooki, G. Dini and M. Mehdikhani, Fabrication of chitosan-coated porous polycaprolactone/strontium-substituted bioactive glass nanocomposite scaffold for bone tissue engineering, *Mater. Sci. Eng., C*, 2019, **105**, 110138.

12 A. Sobczak, Z. Kowalski and Z. Wzorek, Preparation of hydroxyapatite from animal bones, *Acta Bioeng. Biomech.*, 2009, **11**(4), 23–28.

13 N. A. Barakat, K. Khalil, F. A. Sheikh, A. Omran, B. Gaihre, S. M. Khil and H. Y. Kim, Physiochemical characterizations of hydroxyapatite extracted from bovine bones by three different methods: extraction of biologically desirable HAp, *Mater. Sci. Eng., C*, 2008, **28**(8), 1381–1387.

14 H. Kim, C. Rey and M. Glimcher, X-ray diffraction, electron microscopy, and Fourier transform infrared spectroscopy of apatite crystals isolated from chicken and bovine calcified cartilage, *Calcif. Tissue Int.*, 1996, **59**(1), 58–63.

15 K.-J. Jang, W. J. Cho, H. Seonwoo, J. Kim, K. T. Lim, P.-H. Chung and J. H. Chung, Development and characterization of horse bone-derived natural calcium phosphate powders, *J. Biosyst. Eng.*, 2014, **39**(2), 122–133.

16 K.-J. Jang, H. Seonwoo, M. Yang, S. Park, K. T. Lim, J. Kim, P.-H. Choung and J. H. Chung, Development and characterization of waste equine bone-derived calcium phosphate cements with human alveolar bone-derived mesenchymal stem cells, *Connect. Tissue Res.*, 2021, **62**(2), 164–175.

17 J. Zhang, F. Tancret and J.-M. Bouler, Fabrication and mechanical properties of calcium phosphate cements (CPC) for bone substitution, *Mater. Sci. Eng., C*, 2011, **31**(4), 740–747.

18 C. Liu, H. Shao, F. Chen and H. Zheng, Effects of the granularity of raw materials on the hydration and hardening process of calcium phosphate cement, *Biomaterials*, 2003, **24**(23), 4103–4113.

19 M. C. Lee, H. Seonwoo, K. J. Jang, S. Pandey, J. Lim, S. Park, J. E. Kim, Y.-H. Choung, P. Garg and J. H. Chung, Development of novel gene carrier using modified nano hydroxyapatite derived from equine bone for osteogenic differentiation of dental pulp stem cells, *Bioact. Mater.*, 2021, **6**(9), 2742–2751.

20 U. Gbureck, J. E. Barralet, K. Spatz, L. M. Grover and R. Thull, Ionic modification of calcium phosphate cement viscosity. Part I: hypodermic injection and strength improvement of apatite cement, *Biomaterials*, 2004, **25**(11), 2187–2195.

21 K. T. Lim, S. J. Baik, S. W. Kim, J. Kim, H. Seonwoo, J.-W. Kim, P.-H. Choung, Y.-H. Choung and J. H. Chung, Development and characterization of fast-hardening composite cements composed of natural ceramics originated from horse bones and chitosan solution, *Tissue Eng. Regener. Med.*, 2014, **11**(5), 362–371.

22 S. Sarda, E. Fernández, M. Nilsson, M. Balcells and J. Planell, Kinetic study of citric acid influence on calcium phosphate bone cements as water-reducing agent, *J. Biomed. Mater. Res.*, 2002, **61**(4), 653–659.

23 W. Liu, J. Zhang, P. Weiss, F. Tancret and J.-M. Bouler, The influence of different cellulose ethers on both the handling and mechanical properties of calcium phosphate cements for bone substitution, *Acta Biomater.*, 2013, **9**(3), 5740–5750.

24 M. E. Launey and R. O. Ritchie, On the fracture toughness of advanced materials, *Adv. Mater.*, 2009, **21**(20), 2103–2110.

25 K. S. Novoselov, A. K. Geim, S. V. Morozov, D.-e. Jiang, Y. Zhang, S. V. Dubonos, I. V. Grigorieva and A. A. Firsov, Electric field effect in atomically thin carbon films, *Science*, 2004, **306**(5696), 666–669.

26 K. S. Kim, Y. Zhao, H. Jang, S. Y. Lee, J. M. Kim, K. S. Kim, J.-H. Ahn, P. Kim, J.-Y. Choi and B. H. Hong, Large-scale pattern growth of graphene films for stretchable transparent electrodes, *Nature*, 2009, **457**(7230), 706–710.

27 O. Akhavan, E. Ghaderi, H. Emamy and F. Akhavan, Genotoxicity of graphene nanoribbons in human mesenchymal stem cells, *Carbon*, 2013, **54**, 419–431.

28 J. Kim, K. S. Choi, Y. Kim, K. T. Lim, H. Seonwoo, Y. Park, D. H. Kim, P. H. Choung, C. S. Cho and S. Y. Kim, Bioactive effects of graphene oxide cell culture substratum on structure and function of human adipose-derived stem cells, *J. Biomed. Mater. Res., Part A*, 2013, **101**(12), 3520–3530.

29 J. Kim, Y.-R. Kim, Y. Kim, K. T. Lim, H. Seonwoo, S. Park, S.-P. Cho, B. H. Hong, P.-H. Choung and T. D. Chung, Graphene-incorporated chitosan substrata for adhesion and differentiation of human mesenchymal stem cells, *J. Mater. Chem. B*, 2013, **1**(7), 933–938.

30 W. C. Lee, C. H. Y. Lim, H. Shi, L. A. Tang, Y. Wang, C. T. Lim and K. P. Loh, Origin of enhanced stem cell growth and differentiation on graphene and graphene oxide, *ACS Nano*, 2011, **5**(9), 7334–7341.

31 J. Kim, S. Park, Y. J. Kim, C. S. Jeon, K. T. Lim, H. Seonwoo, S.-P. Cho, T. D. Chung, P.-H. Choung and Y.-H. Choung, Monolayer graphene-directed growth and neuronal differentiation of mesenchymal stem cells, *J. Biomed. Nanotechnol.*, 2015, **11**(11), 2024–2033.

32 S. Y. Park, J. Park, S. H. Sim, M. G. Sung, K. S. Kim, B. H. Hong and S. Hong, Enhanced differentiation of human neural stem cells into neurons on graphene, *Adv. Mater.*, 2011, **23**(36), H263–H267.

33 R. Tatavarty, H. Ding, G. Lu, R. J. Taylor and X. Bi, Synergistic acceleration in the osteogenesis of human mesenchymal stem cells by graphene oxide–calcium phosphate nanocomposites, *Chem. Commun.*, 2014, **50**(62), 8484–8487.

34 X. Yang, Y. Tu, L. Li, S. Shang and X.-m. Tao, Well-dispersed chitosan/graphene oxide nanocomposites, *ACS Appl. Mater. Interfaces*, 2010, **2**(6), 1707–1713.

35 Z. Fan, J. Wang, Z. Wang, H. Ran, Y. Li, L. Niu, P. Gong, B. Liu and S. Yang, One-pot synthesis of graphene/hydroxyapatite nanorod composite for tissue engineering, *Carbon*, 2014, **66**, 407–416.

36 S. Baradaran, E. Moghaddam, W. J. Basirun, M. Mehrali, M. Sookhakian, M. Hamdi, M. N. Moghaddam and Y. Alias, Mechanical properties and biomedical applications of a nanotube hydroxyapatite-reduced graphene oxide composite, *Carbon*, 2014, **69**, 32–45.

37 K. T. Lim, H. Seonwoo, K. S. Choi, H. Jin, K. J. Jang, J. Kim, J. W. Kim, S. Y. Kim, P. H. Choung and J. H. Chung, Stem Cell Substrates: Pulsed-Electromagnetic-Field-Assisted Reduced Graphene Oxide Substrates for Multidifferentiation of Human Mesenchymal Stem Cells, *Adv. Healthcare Mater.*, 2016, **5**(16), 2144.

38 K.-T. Lim, J. Hexiu, D. K. Patel, J. Kim, H. Seonwoo and J. H. Chung, Evaluation of the Osteogenic Potential of Stem Cells in the Presence of Growth Hormone under Magnetic Field Stimulation, *ACS Biomater. Sci. Eng.*, 2020, **6**(7), 4141–4154.

39 H. Seonwoo, Development of Graphene-Reinforced Bone Cements and Characteristics of Graphene-Based Platform with Electromagnetic Field, Seoul National University Graduate School, 2016.

40 H. Seonwoo, K. J. Jang, S. Jung, M. C. Lee and J. H. Chung, Graphene-Incorporated Bone Cements for Bone Regeneration, *J. Biosyst. Eng.*, 2015, **20**(2), 271.

41 X. Wang and J. Ye, Variation of crystal structure of hydroxyapatite in calcium phosphate cement by the substitution of strontium ions, *J. Mater. Sci.: Mater. Med.*, 2008, **9**(3), 1183–1186.

42 S. Park, J. An, J. R. Potts, A. Velamakanni, S. Murali and R. S. Ruoff, Hydrazine-reduction of graphite- and graphene oxide, *Carbon*, 2019, **49**(9), 3019–3023.

43 M. Li, Y. Wang, Q. Liu, Q. Li, Y. Cheng, Y. Zheng, T. Xi and S. Wei, In situ synthesis and biocompatibility of nano hydroxyapatite on pristine and chitosan functionalized graphene oxide, *J. Mater. Chem. B*, 2013, **1**(4), 475–484.

44 R. Tatavarty, H. Ding, G. Lu, R. J. Taylor and X. Bi, Synergistic acceleration in the osteogenesis of human mesenchymal stem cells by graphene oxide–calcium phosphate nanocomposites, *Chem. Commun.*, 2014, **50**(62), 8484–8487.

45 W. Thein-Han, J. Liu and H. H. Xu, Calcium phosphate cement with biofunctional agents and stem cell seeding for dental and craniofacial bone repair, *Dent. Mater.*, 2012, **28**(10), 1059–1070.

46 J. Aubin, F. Liu, L. Malaval and A. Gupta, Osteoblast and chondroblast differentiation, *Bone*, 1995, **17**(2), S77–S83.

47 K. Lim, J. Hexiu, J. Kim, H. Seonwoo, W. J. Cho, P.-H. Choung and J. H. Chung, Effects of electromagnetic fields on osteogenesis of human alveolar bone-derived mesenchymal stem cells, *BioMed Res. Int.*, 2013, **2013**, 1–14.

48 G. Gonçalves, S. M. Cruz, A. Ramalho, J. Grácio and P. A. Marques, Graphene oxide versus functionalized carbon nanotubes as a reinforcing agent in a PMMA/HA bone cement, *Nanoscale*, 2012, **4**(9), 2937–2945.

49 H. Zanin, E. Saito, F. R. Marciano, H. J. Ceragioli, A. E. C. Granato, M. Porcionatto and A. O. Lobo, Fast preparation of nano-hydroxyapatite/superhydrophilic reduced graphene oxide composites for bioactive applications, *J. Mater. Chem. B*, 2013, **1**(38), 4947–4955.

50 J. H. Lee, Y. C. Shin, S.-M. Lee, O. S. Jin, S. H. Kang, S. W. Hong, C.-M. Jeong, J. B. Huh and D.-W. Han, Enhanced osteogenesis by reduced graphene oxide/hydroxyapatite nanocomposites, *Sci. Rep.*, 2015, **5**(1), 1–13.

51 O. V. Yazyev and M. Katsnelson, Magnetic correlations at graphene edges: basis for novel spintronics devices, *Phys. Rev. Lett.*, 2008, **100**(4), 047209.